IOP PUBLISHING NONLINEARITY

Nonlinearity **23** (2010) 475–493 doi:10.1088/0951-7715/23/3/002

Study of the noise-induced transition and the exploration of the phase space for the Kuramoto–Sivashinsky equation using the minimum action method

X Wan[1], **X Zhou**[2] **and W E**[2,3]

[1] Department of Mathematics, Louisiana State University, Baton Rouge, LA 70803, USA
[2] Program in Applied and Computational Mathematics, Princeton University, Princeton, NJ 08544, USA
[3] Department of Mathematics, Princeton University, Princeton, NJ 08544, USA

E-mail: xlwan@math.lsu.edu, xiangz@math.princeton.edu and weinan@math.princeton.edu

Received 26 July 2009
Published 19 January 2010
Online at stacks.iop.org/Non/23/475

Recommended by D Dolgopyat

Abstract
Noise-induced transition in the solutions of the Kuramoto–Sivashinsky (K–S) equation is investigated using the minimum action method derived from the large deviation theory. This is then used as a starting point for exploring the configuration space of the K–S equation. The particular example considered here is the transition between a stable fixed point and a stable travelling wave. Five saddle points, up to constants due to translational invariance, are identified based on the information given by the minimum action path. Heteroclinic orbits between the saddle points are identified. Relations between noise-induced transitions and the saddle points are examined.

Mathematics Subject Classification: 82C35, 82C26, 34F05, 60H15

1. Introduction

Dynamical systems are often subject to random perturbations since noise is ubiquitous in nature. Even though these random perturbations have a small amplitude, they can produce a profound effect on the long time dynamics by inducing rare but important events. A large number of interesting phenomena in physics, chemistry and biology such as phase transitions, biological switches and chemical reactions are examples of such noise-induced rare events [1, 2].

The purpose of studying noise-induced transition is to answer questions such as how the transitions occur and how frequent they are. The transition pathways between metastable sets in a dynamical system often have a rather deterministic nature. As the noise amplitude

decreases to zero, the distribution of the trajectories that make successful transitions between metastable sets is often sharply peaked around a certain deterministic path or a set of paths: the most probable transition paths or optimal transition paths. Special features of such paths tell us crucial information about the mechanism of the transition. One class of examples that have been well studied for a long time are the gradient systems, for which the vector field is the gradient of a potential function. This subject is also associated with the exploration of the energy landscape for such systems [3]. In gradient systems, the most probable transition path is the minimum energy path (MEP). The MEP passes through the basin boundary between the stable states at some saddle points with one-dimensional unstable manifold (we call them index-1 saddle points or first-order saddle point) and carry the least energy on the boundary [4, 5]. Such index-1 saddles with least energy are also called 'transition states' in the chemical physics [3].

A large number of algorithms have been designed to find such transition states in gradient systems. Some popular algorithms include the string method [6, 7], nudged elastic band method [8], eigenvector-following-type method (e.g. [9]) as well as the dimer method [10]. As an application, the string method was used in [11] to study the complex dynamics of thermally activated switching of submicro-sized ferromagnetic elements. A network was obtained there with the nodes being the stable states and the transition states and the edges being the MEPs. The noise-induced transitions in the configuration space can be modelled as a Markov chain on that network.

However, the understanding of transition events in non-gradient systems is much less satisfactory. The configuration space may display a much more complicated structure, where invariant sets can be fixed points, as well as limit cycles, tori or even chaotic strange attractors. The same can be said about the transition states. We refer to [12, 13] for the study of a prototypical system: the Lorenz system.

In this paper, we study the one-dimensional Kuramoto–Sivashinsky (K–S) equation [14, 15], as an infinite dimensional example. This is one of the simplest spatially extended nonlinear systems of physical interest. It was derived in 1970s by Kuramoto [14] and Sivashinsky [15]. Holmes *et al* [16] provided a delightful discussion of why this system is a good model problem for studying turbulence in the full-fledged Navier–Stokes boundary shear flows. As the system size is increased, the solution of K–S equation undergoes a complex bifurcation sequence including fixed points, travelling waves, invariant tori and homoclinic orbits [17] on the route of transition to chaos. In this paper, we limit our effort to one relatively simple case where one stable fixed point and one stable travelling wave coexist. We are going to address the following questions.

(i) How does the transition occur between the stable fixed point and the stable travelling wave if the K–S equation is randomly perturbed by weak additive white noise?
(ii) What are the saddle points or sets that might be involved in the transition, i.e. what are the transition states?
(iii) How do these invariant sets connect to each other through their stable and unstable manifolds?

Based on answers to the above questions, we construct a network (see figure 12) connected by heteroclinic orbits to indicate the relationship between the attractors, transition states and other saddle points, and thereby present a global optimal transition path between the two attractors. Thus, we are able to capture part of the skeleton of the high dimensional dynamics.

The numerical tool used here is the minimum action method (MAM) originally proposed in [18]. This numerical method roots in the rigorous mathematical theory, the Freidlin–Wentzell large deviation theory [19] of random dynamical systems. The path in the phase space given by the MAM is called the minimum action path (MAP) since it is the minimizer

of the Freidlin–Wentzell action functional. In this paper, we use the adaptive version [20] of the original MAM (aMAM). Although for the high dimensional, nonlinear and non-gradient systems, the MAP obtained from the MAM can in principle be simply a local minimum of the Freidlin–Wentzell action functional due to the existence of heteroclinic connections between fixed points, the obtained MAP can still allow us to extract important information about the phase space since it can provide information about the locations of saddle points. In addition, the MAM can help to confirm or disprove the existence of heteroclinic orbits between known saddle points.

The paper is organized as follows. The background about K–S equation and MAM is reviewed in section 2. In section 3, we develop related numerical algorithms. Numerical results are given in section 4, followed by a discussion in section 5.

2. Theoretical background

We consider a random process $X_t = X(t) : \mathbb{R}_+ \to \mathbb{R}^d$ defined by the following stochastic ordinary differential equation (SODE):

$$\mathrm{d}X_t = b(X_t)\,\mathrm{d}t + \sqrt{\varepsilon}\,\mathrm{d}W_t, \tag{1}$$

where W_t is a standard Wiener process in $\mathbb{R}^d$. Let $\phi(t) \in \mathbb{R}^d$ be an absolutely continuous function defined on $t \in [0, T]$. The Wentzell–Freidlin theory [19] tells us that the probability of $X(t)$ passing through the δ-tube about ϕ on $[0, T]$ is

$$\Pr(\rho(X, \phi) < \delta) \approx \exp\left(-\frac{1}{\varepsilon} S_T(\phi)\right), \tag{2}$$

where $\rho(\phi, \varphi) = \sup_{t\in[0,T]} |\phi(t) - \varphi(t)|$ and $S_T(\phi)$ is the action functional of ϕ on $[0, T]$, defined as

$$S_T(\phi) = \frac{1}{2}\int_0^T \|\dot{\phi} - b(\phi)\|^2\,\mathrm{d}t. \tag{3}$$

In general, we have the following large deviation principle [19, 21]

$$\lim_{\varepsilon\to 0} \varepsilon \log \Pr(X \in A) = -\min_{\phi\in A} S_T(\phi), \tag{4}$$

where A is a particular set of random events. For example, A can be defined as

$$A = \{X(0) = a_1, X(T) = a_2\}$$

if we are interested in the probability of $X(t)$ connecting one point a_1 and the other point a_2 in the phase space. For such a problem, the minimizer ϕ^*, which satisfies $S_T(\phi^*) = \min_{\phi\in A} S_T(\phi)$, is the most probable path for the transition from a_1 to a_2 in the sense that the probability of the system taking all the other paths decays exponentially with respect to the noise amplitude ε according to the large deviation principle. The minimizer ϕ^* is also called the 'minimum action path' (MAP).

In this work, we examine such a transition problem for the one-dimensional stochastic K–S equation:

$$\begin{cases} u_t + \nu u_{xxxx} + u_{xx} + \frac{1}{2}(u_x)^2 = \sqrt{\varepsilon}\dot{W}(x, t), & (x, t) \in (0, L) \times \mathbb{R}_+, \\ u(x, 0) = u_0(x), \qquad u(x + L, t) = u(x, t), \end{cases} \tag{5}$$

where ν and ε are positive numbers, $u_0(x)$ is L-periodic and $\dot{W}(x, t)$ is a space-time Gaussian white noise.

2.1. Overview of the K–S equation

We first normalize the deterministic K–S equation as

$$\begin{cases} u_t + 4u_{xxxx} + \alpha[u_{xx} + \frac{1}{2}(u_x)^2] = 0, & (x,t) \in (0, 2\pi) \times \mathbb{R}_+, \\ u(x,0) = u_0(x), & u(x,t) = u(x + 2\pi, t), \end{cases} \tag{6}$$

where ν is set to 4, and the bifurcation parameter $\alpha = 4\tilde{L}^2$ with $\tilde{L} = L/(2\pi\sqrt{\nu})$. Equations (6) are characterized by a second-order *negative diffusion* (due to the sign of the Laplacian), a fourth-order stabilizing term and a quadratic nonlinear coupling term. For example, the trivial solution $u \equiv 0$ is a global attractor when $\alpha \leqslant 4$, and becomes unstable as soon as the bifurcation parameter α is larger than 4. This is reflected in the spectrum of (6) linearized at $u = 0$, where the eigen-functions are the $\exp(\mathrm{i}kx)$, $k \in \mathbb{Z}$, and the sequence of eigenvalues is

$$\Lambda_k = \alpha k^2 - 4k^4.$$

When α is large enough, the K–S equation will exhibit temporal chaos. On the other hand, the existence of a unique compact inertial manifold was established in [22]. Thus, the solution of the K–S equation is characterized by the coexistence of coherent spatial structures with complex temporal dynamics. Since the mean mode

$$\bar{u}(t) = \frac{1}{2\pi}\int_0^{2\pi} u(x,t)\,\mathrm{d}x$$

is unbounded, we consider the equation for $v(x,t) = u(x,t) - \bar{u}(t)$ for convenience [17]:

$$v_t + 4v_{xxxx} + \alpha[v_{xx} + \tfrac{1}{2}(v_x)^2] + \dot{\bar{u}}(t) = \sqrt{\varepsilon}\dot{W}, \tag{7}$$

where

$$\dot{\bar{u}}(t) = \frac{-\alpha}{4\pi}\int_0^{2\pi} (u_x)^2\,\mathrm{d}x = \frac{-\alpha}{4\pi}\int_0^{2\pi} (v_x)^2\,\mathrm{d}x.$$

Due to the even-order spatial derivatives and quadratic nonlinearity, the K–S equation is invariant with respect to translation and reflection. If $v(x,t)$ is a solution, then $\tau_c v(x,t) = v(x + c, t)$ with $c \in [0, 2\pi)$ and $Rv(x) = v(-x)$ are equivalent solutions. Given a solution $v(x,t)$, we denote its equivalent solutions due to translational invariance as

$$\tau(v) = \{\tau_c v | 0 \leqslant c < 2\pi\}, \tag{8}$$

and all its equivalent solutions as

$$G(v) = \tau(v) \cup \{R\tau_c v | 0 \leqslant c < 2\pi\}. \tag{9}$$

2.2. Transitions and the MAM

We assume there exist two stable states $v_+(x)$ and $v_-(x)$ in the phase space, which are not equivalent solutions. Then, there is a finite probability in any time interval $[0, T]$ that the system switches from $G(v_+)$ to $G(v_-)$ under the small white noise perturbation. From the large deviation theory, the probability of transition satisfies

$$\lim_{\varepsilon\to 0} \varepsilon \log \Pr(\{\omega : v \text{ switches from } G(v_+) \text{ to } G(v_-)\}) = -\min_T \min_{v\in B} S_T(v), \tag{10}$$

where $v \in B$ satisfies the following constraints

$$v(x,0) \in G(v_+), \qquad v(x,T) \in G(v_-), \qquad v(0,t) = v(L,t), \tag{11}$$

and $S_T(v)$ is the corresponding action functional for the stochastic K–S equation (7), defined as

$$S_T(v) = \frac{1}{2}\int_0^T \int_0^L \left(v_t + 4v_{xxxx} + \alpha\left[v_{xx} + \frac{1}{2}(v_x)^2\right] + \dot{\bar{u}}\right)^2 \mathrm{d}x\,\mathrm{d}t. \tag{12}$$

The MAP constrained by (11) is from one set to another set. Although each stable state in $G(v_+)$ and $G(v_-)$ has their own basin of attraction, we are not interested in transitions within $G(v_+)$ or $G(v_-)$. Note here that since both $G(v_+)$ and $G(v_-)$ are stable states, we can redefine the problem on time interval $(-\infty, +\infty)$ instead of $[0, T]$.

3. Numerical algorithms

3.1. Finite-dimensional approximation

We project $v(x, t)$ onto a finite-dimensional subspace, B_N, defined as

$$B_N = \text{span}\{e^{inx} || n| \leqslant N/2\}, \qquad \dim(B_N) = N + 1.$$

Let $\mathcal{P}_N$ indicate the projection operator. With a Galerkin projection onto B_N, equation (7) corresponds to an ODE system

$$\frac{d\tilde{\boldsymbol{v}}}{dt} = \mathcal{P}_N \boldsymbol{L}(\tilde{\boldsymbol{v}}) + \mathcal{P}_N \boldsymbol{N}(\tilde{\boldsymbol{v}}, t), \tag{13}$$

where $\tilde{\boldsymbol{v}} \in \mathbb{C}^N$ indicates the Fourier coefficients of $v(x, t)$, $\mathcal{P}_N \boldsymbol{L}(\tilde{\boldsymbol{v}}) = (\alpha k^2 - 4k^4)\tilde{v}_k$ the projection of the linear operator $\boldsymbol{L}(v) = -4v_{xxxx} - \alpha v_{xx}$ and $\mathcal{P}_N \boldsymbol{N}(\tilde{\boldsymbol{v}}, t)$ the projection of the nonlinear operator $\boldsymbol{N}(v) = -(\alpha/2)v_x^2 - \dot{\bar{u}}(t)$. We note that $\tilde{\boldsymbol{v}}$ belongs to $\mathbb{C}^N$ instead of $\mathbb{C}^{N+1}$ since we have subtracted the mean mode. Correspondingly, the translation operator is defined as $\tau_c(\tilde{\boldsymbol{v}}) = \text{diag}(e^{ikc})\tilde{\boldsymbol{v}}$ and the reflection operator as $R(\tilde{\boldsymbol{v}}) = \bar{\tilde{\boldsymbol{v}}}$, i.e., the conjugate of $\tilde{\boldsymbol{v}}$.

Reference [17] shows that the finite-dimensional subspace B_N with $N \geqslant 32$ can successfully capture the dynamics of the K–S equation. In our work, we use $N = 32$. From now on, we will study the following stochastic ODE system

$$d\tilde{\boldsymbol{v}} = (\mathcal{P}_N \boldsymbol{L}(\tilde{\boldsymbol{v}}) + \mathcal{P}_N \boldsymbol{N}(\tilde{\boldsymbol{v}}, t))\, dt + \sqrt{\varepsilon}\, dW_t, \tag{14}$$

where $W_t \in \mathbb{R}^n$ is a standard n-dimensional Wiener process. When necessary, equation (13) will be solved using the exponential time differencing (ETD) method coupled with the fourth-order Runge–Kutta scheme [23], see the appendix.

We note that if the pseudo-spectral method is employed, $\mathcal{P}_N \boldsymbol{N}(\tilde{\boldsymbol{v}}, t)$ can be approximated as $\mathcal{P}_N \boldsymbol{N}(\tilde{\boldsymbol{v}}, t) \approx \boldsymbol{F}((\boldsymbol{F}^{-1}(ik\tilde{\boldsymbol{v}}))^2 - \overline{(\boldsymbol{F}^{-1}(ik\tilde{\boldsymbol{v}}))^2})$ with $\boldsymbol{F}$ being the Fourier transform. Since we are more interested in the geometry of the phase space instead of the efficiency of numerical computation of PDE solver, we use the standard Galerkin projection of $\mathcal{P}_N \boldsymbol{N}(\tilde{\boldsymbol{v}})$ whenever needed in this paper, in other words, we derive $\mathcal{P}_N \boldsymbol{N}(\tilde{\boldsymbol{v}})$ explicitly.

For numerical convenience, we will consider a vector consisting of real components. Given $\tilde{\boldsymbol{v}}$, we have a corresponding expansion of $v(x, t)$ in the form

$$v(x, t) \approx \sum_{k=1}^{N/2} a_k \cos(kx) + b_k \sin(kx).$$

Let $\hat{\boldsymbol{v}} = (a_1, \ldots, a_{N/2}, b_1, \ldots, b_{N/2})$. There exists a one-to-one correspondence between $\hat{\boldsymbol{v}}$ and $\tilde{\boldsymbol{v}}$.

3.2. Parallel minimal action method

Corresponding to the SODE system (14), we obtain the following semi-discrete optimization problem:

$$\hat{\boldsymbol{v}}^*(t) = \min_{\hat{\boldsymbol{v}} \in B} S_N(\hat{\boldsymbol{v}}(t)) = \min_{\hat{\boldsymbol{v}} \in B} \frac{1}{2} \int_{-\infty}^{+\infty} \| \dot{\hat{\boldsymbol{v}}} - \mathcal{P}_N \boldsymbol{L}(\hat{\boldsymbol{v}}) - \mathcal{P}_N \boldsymbol{N}(\hat{\boldsymbol{v}}) \|_2^2 \, dt, \tag{15}$$

where $\hat{\boldsymbol{v}}(t) \in B$ are $\mathbb{R}^N$-valued continuous functions subject to the constraints

$$\hat{\boldsymbol{v}}(-\infty) \in G(\hat{\boldsymbol{v}}_+), \qquad \hat{\boldsymbol{v}}(+\infty) \in G(\hat{\boldsymbol{v}}_-). \tag{16}$$

We employ the adaptive minimum action method (aMAM) [20] to solve the optimization problem (15) numerically. We subsequently present the numerical method using the constraints

$$\hat{\boldsymbol{v}}(-\infty) = \hat{\boldsymbol{v}}_+, \qquad \hat{\boldsymbol{v}}(+\infty) = \hat{\boldsymbol{v}}_-, \tag{17}$$

which is from one point to another one in the phase space. We will discuss the strategy for equivalent solutions in section 3.3. For numerical computation, we need to replace the time interval $(-\infty, +\infty)$ with a finite one $[0, T]$. It was shown in [20] that the numerical error of MAP will decay fast (nearly exponentially) as T increases. We then use the midpoint rule to discretize $S_N(\hat{\boldsymbol{v}})$ for a temporal mesh of $[0, T]$. To this end, given a temporal mesh

$$\boldsymbol{T} := 0 = t_0 < t_1, \ldots, < t_{n+1} = T,$$

we define a discrete path in the phase space as

$$\hat{\hat{\boldsymbol{v}}} = [\hat{\boldsymbol{v}}(t_0),\ \hat{\boldsymbol{v}}(t_1), \ldots, \hat{\boldsymbol{v}}(t_n),\ \hat{\boldsymbol{v}}(t_{n+1})] \in \mathbb{R}^{N\times(n+2)},$$

where $\hat{\boldsymbol{v}}_{t_0} = \hat{\boldsymbol{v}}_+$ and $\hat{\boldsymbol{v}}_{t_{n+1}} = \hat{\boldsymbol{v}}_-$. We then obtain the discrete form of $S_N(\hat{\boldsymbol{v}}(t))$ as

$$S_N(\hat{\boldsymbol{v}}(t)) \approx S_N(\hat{\hat{\boldsymbol{v}}}) = \frac{1}{2}\sum_{i=1}^{n+1} \left\| \frac{\hat{\boldsymbol{v}}(t_i) - \hat{\boldsymbol{v}}(t_{i-1})}{\Delta t_i} - \mathcal{P}_N \boldsymbol{L}(\hat{\boldsymbol{v}}(t_{i-1/2})) - \mathcal{P}_N \boldsymbol{N}(\hat{\boldsymbol{v}}(t_{i-1/2})) \right\|_2^2 \Delta t_i,$$

where $\Delta t_i = t_i - t_{i-1}$ and $\hat{\boldsymbol{v}}(t_{i-1/2}) = (\hat{\boldsymbol{v}}(t_i) + \hat{\boldsymbol{v}}(t_{i-1}))/2$.

The fully discrete optimization problem will be iterated by a preconditioned nonlinear conjugate gradient (CG) method [24]:

$$\begin{cases} \hat{\hat{\boldsymbol{v}}}_{k+1} = \hat{\hat{\boldsymbol{v}}}_k + \alpha_k \boldsymbol{d}_k, \\ \boldsymbol{d}_{k+1} = P\boldsymbol{g}_k + \beta_k \boldsymbol{d}_k, \qquad \boldsymbol{d}_0 = -P\boldsymbol{g}_0, \end{cases} \tag{18}$$

where the subscript k indicates the iteration step, the positive step size α_k is obtained by a line search algorithm, β_k is the CG update parameter chosen as in [24] and $\boldsymbol{g}_k = \nabla S_N(\hat{\hat{\boldsymbol{v}}}_k)$. The preconditioner P is given by the inverse of the linear part of the Euler–Lagrange equation corresponding to the action functional, i.e. $(-\partial_t^2 + \alpha^2\partial_x^4 + 8\alpha\partial_x^6 + 16\partial_x^8)^{-1}$, which can be regarded as an approximation of the Hessian matrix of the nonlinear function to be optimized. Due to the midpoint finite difference used in temporal discretization and the Fourier expansion in physical space, P^{-1} is a tridiagonal symmetric matrix.

To improve the accuracy, aMAM will check the quality of temporal mesh corresponding to $\hat{\hat{\boldsymbol{v}}}_k$, and adjust the grids t_i *on-the-fly* using a moving mesh technique when the quality measure is larger than a prescribed threshold [20]. The final temporal mesh will result in nearly equidistant grids with respect to the arc-length along the MAP. Corresponding to the midpoint rule, second-order accuracy $O(n^{-2})$ will be obtained, where n is the number of grids points in the temporal mesh.

In particular, we develop a parallel aMAM to speed up the convergence. The main reason for parallel computation is that the problem is ill-conditioned and a large number of iterations are needed. It is not difficult to roughly estimate the condition number from the linear part the Euler–Lagrange equation, which is $O(10^8)$ if $N = 32$. The philosophy for parallelization is simple. We only do the parallelization along the time direction. Suppose the number of unknowns is $N \times n$ and the number of processors is m. We assign the temporal mesh $\boldsymbol{T}$ (almost) evenly to the m processors. Each processor has about $N \times \frac{n}{m}$ unknowns. Due to the midpoint rule, the main communication between adjacent processors is the exchange of data at the boundaries of local temporal mesh. Another operation affected by the parallelization is

the computation of preconditioner, where we need to inverse a tridiagonal matrix. We employ the functions `pddttrf` and `pddttrs` in the package ScaLAPACK to deal with such an issue. Based on such a parallelization strategy, a good scalability is achieved.

3.3. The equivalent solutions

In (16), we constrain the MAP from one set $G(v_+)$ to another set $G(v_-)$ due to the symmetries of the K–S equation. The reflection R is the discrete symmetry and we can treat v and Rv as two separate states; the translational invariance is the continuous symmetry and we are faced with a set $\tau(v)$ of states characterized by one continuous parameter c. Thus, for simplicity, in this paper, we only consider the continuous symmetry and the transitions between two sets of translational images. In other words, we need to integrate the description of a set into the optimization algorithm. The constraints in equation (16) become

$$\hat{v}(-\infty) = \tau_{c_+}\hat{v}_+ \in \tau(\hat{v}_+), \qquad \hat{v}(+\infty) = \tau_{c_-}\hat{v}_- \in \tau(\hat{v}_-). \tag{19}$$

Since both $\tau(\hat{v}_+)$ and $\tau(\hat{v}_-)$ are one-parameter families of stable states, we only need to take into account two parameters c_+ and c_-, in the translations between $\tau_{c_+}\hat{v}_+$ and $\tau_{c_-}\hat{v}_-$. We treat parameters c_+ and c_- as regular unknowns in the optimization algorithm, which results in $N \times n + 2$ unknowns. This is the general strategy to deal with MAPs from set to set with continuous parameters.

We note that the Wentzell–Freidlin action functional (12) inherits the translational invariance of the K–S equation because we impose the periodic boundary condition. Thus the solutions corresponding to (19) also have translational invariance: if $\phi(x, t)$ is a MAP from v_+ to v_-, then for any constant c, $\phi(x + c, t)$ is also a MAP, but from $\tau_c v_+$ to $\tau_c v_-$. The simple way to eliminate this translational invariance of MAPs is just to fix one of the two free parameters c_+ or c_-.

Equation (13) has two types of stable solutions: fixed points and periodic orbits. At $\alpha = 52$, the periodic orbit corresponds to a travelling wave. Assume $\hat{v}_{\mathrm{F}}(x)$ is a fixed point and $\hat{v}_{\mathrm{TW}}(x)$ is one arbitrary point on a travelling wave. Then $\tau_c\hat{v}_{\mathrm{F}}$ is also a fixed point and both $\tau(\hat{v}_{\mathrm{F}})$ and $\tau(\hat{v}_{\mathrm{TW}})$ are invariant sets of equation (13). But the situation can be different if we consider the existence of connecting orbits between any two points in $\tau(\hat{v}_{\mathrm{F}})$ or between any two points in $\tau(\hat{v}_{\mathrm{TW}})$. If $\hat{v}_{\mathrm{F}}$ is stable, there does not exist dynamics between any two points in the invariant set $\tau(\hat{v}_{\mathrm{F}})$. In other words, the action functional between any two points in $\tau(\hat{v}_{\mathrm{F}})$ is not zero for any $T > 0$. However, if $\hat{v}_{\mathrm{F}}$ is of saddle type, there might exist homoclinic orbits between $\hat{v}_{\mathrm{F}}$ and $\tau_c\hat{v}_{\mathrm{F}}$. Note that if both ends, $\hat{v}_+$ and $\hat{v}_-$ are saddle points and there exists a heteroclinic orbit from $\hat{v}_+$ to $\hat{v}_-$, the MAP should be exactly the heteroclinic orbit, along which the action functional is zero.

For the travelling wave $\hat{v}_{\mathrm{TW}}$, the situation is different. A spatial translation $v((x+c)+c_v t)$ can be transformed to a temporal translation as $v(x + c_v(t + (c/c_v)))$. Correspondingly, there always exists a trajectory between $\hat{v}_{\mathrm{TW}}(T)$ and $\tau_c\hat{v}_{\mathrm{TW}}(T)$ for any c, along which the action functional is zero. Thus if we use the travelling wave as one end of the MAP, we can just pick up one point on the periodic orbit of the travelling wave without including the extra degree of freedom for the translational invariance.

In summary, for the transitions between $\tau(\hat{v}_{\mathrm{F}})$ and $\tau(\hat{v}_{\mathrm{TW}})$ treated here, we can consider a simple strategy by looking for the MAP from any point $\tau_c\hat{v}_{\mathrm{F}}$ to an arbitrary point on the travelling wave. In this way, we are able to consider a MAP which is point to point instead of set to set.

Remark 1. There are many ways to eliminate the symmetries of the K–S equation by choosing a constrained subspace. However, the solutions in such subspaces are not necessarily generic

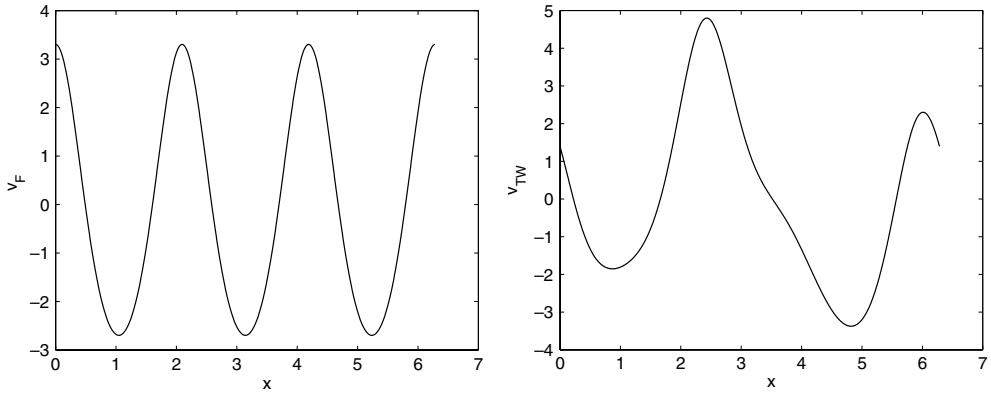

Figure 1. Profiles of the attractors. Left: fixed point, $v_{\mathrm{F}}(x)$; right: travelling wave, $v_{\mathrm{TW}}(x+ct)$.

and any perturbation can move the solution out of these subspaces. We cannot guarantee that the MAP also stays in the chosen subspace, and should consider the full space for the optimization problem (15).

4. Numerical results

4.1. Two attractors at $\alpha = 52$

According to the numerical study in [17], there exist two types of attractors when $50 \leqslant \alpha \leqslant 54$: one is a fixed point $v_{\mathrm{F}}(x)$ and the other one is a travelling wave $v_{\mathrm{TW}}(x+ct)$. In this work, we focus on the case when $\alpha = 52$, and study the transition between these two types of attractors induced by the small white noise perturbation. In particular we consider the optimization problem (15) subject to the constraints

$$\hat{v}(0) = \tau_c \hat{v}_{\mathrm{F}} \in \tau(\hat{v}_{\mathrm{F}}), \quad \hat{v}(T) = \hat{v}_{\mathrm{TW}} \qquad \text{or} \qquad \hat{v}(0) = \hat{v}_{\mathrm{TW}}, \quad \hat{v}(T) = \tau_c \hat{v}_{\mathrm{F}} \in \tau(\hat{v}_{\mathrm{F}}),$$

where $\hat{v}_{\mathrm{TW}}$ is an arbitrary point on a well-developed travelling wave. If no *a priori* knowledge is available about the MAP, the linear interpolation between $\hat{v}_{\mathrm{F}}$ and $\hat{v}_{\mathrm{TW}}$ defined on a uniform temporal mesh will be used as the initial state of the MAP, i.e. if the MAP is from $\hat{v}_{\mathrm{F}}$ to $\hat{v}_{\mathrm{TW}}$, the initial path $\hat{\hat{v}}_0 = [\hat{v}_0(t_1), \ldots, \hat{v}_0(t_n)]$ takes the form

$$\hat{v}_0(t_i) = \hat{v}_{\mathrm{F}} + \frac{i}{n+1}(\hat{v}_{\mathrm{TW}} - \hat{v}_{\mathrm{F}}), \qquad t_i = \frac{i}{n+1}T. \tag{20}$$

When $\alpha = 52$, it was reported in [17] that $v_{\mathrm{F}}(x)$ has a trimodal form

$$v_{\mathrm{F}}(x) = 2.9817\cos(3x) + 0.3019\cos(6x) + 0.0190\cos(9x) + \ldots,$$

where coefficients for all the sine modes are zero. Profiles of $v_{\mathrm{F}}(x)$ and $v_{\mathrm{TW}}(x+ct)$ are shown in figure 1. From now on, we use $\hat{v}_{\mathrm{F}}$ to indicate the trimodal form of the stable fixed point.

4.2. Experiment I—from v_{F} to v_{TW}

We first examine the transition from the stable fixed point to the stable travelling wave, which means that the constraints for the optimization problem (15) are $\hat{v}(0) \in \tau(\hat{v}_{\mathrm{F}})$ and $\hat{v}(T) \in \tau(\hat{v}_{\mathrm{TW}})$. Assume that $\hat{v}_{\mathrm{F}}$ and $\hat{v}_{\mathrm{TW}}$ correspond to the profiles in figure 1. We implement the strategy discussed in section 3.3 and consider the simplified constraints $\hat{v}(0) = \hat{v}_{\mathrm{F}}$ and $\hat{v}(T) = \hat{v}_{\mathrm{TW}}$, which corresponds to a point-to-point MAP.

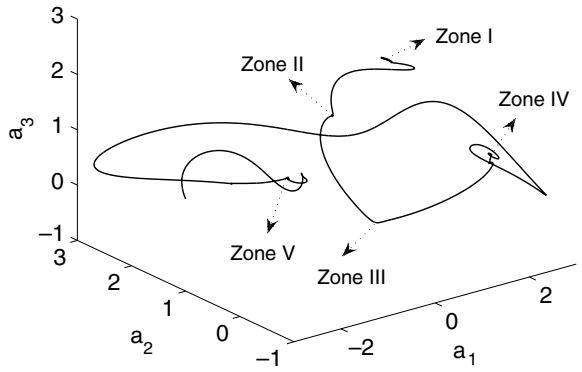

Figure 2. MAP from $\hat{v}_{\mathrm{F}}$ to $\hat{v}_{\mathrm{TW}}$ discretized by 3000 points in time interval [0, 30].

We set $N = 32$ and use 3000 points to discretize the MAP in the time interval $[0, T = 30]$. Using the first three cosine modes, the obtained MAP $\hat{v}^*(t)$ is plotted in figure 2, where $\hat{v}_{\mathrm{F}}$ is the top end. In figure 4, we plot the energy $\|\hat{v}^*(s)\|^2$ on the right and $\|\mathcal{P}_N \boldsymbol{L}(\hat{v}(s)) + \mathcal{P}_N \boldsymbol{N}(\hat{v}(s))\|$ and $\|\dot{\hat{v}}(s) - \mathcal{P}_N \boldsymbol{L}(\hat{v}(s)) - \mathcal{P}_N \boldsymbol{N}(\hat{v}(s))\|$ on the left, along the MAP, where s indicates the arc-length along the MAP.

The MAP provides the following information immediately.

(i) There may exist saddle points in the region where the value of $\|\mathcal{P}_N \boldsymbol{L}(\hat{v}(s)) + \mathcal{P}_N \boldsymbol{N}(\hat{v}(s))\|$ is close to zero. We identify and order such regions as zones I–V, which are marked by ellipses in figure 4. Although it is difficult for the optimization algorithm to precisely locate the fixed points, the points in zones I–V of MAP indeed provide good *initial guesses* for fixed point finding algorithms such as the Newton–Raphson method to find fixed points with a high accuracy. Such important local information about the locations of saddle points is usually not easy to obtain in a high dimensional phase space. Due to the translational invariance, all fixed points are up to a constant.

(ii) We note that the residual term (or noise momentum term), $\|\dot{\hat{v}}(s) - \mathcal{P}_N \boldsymbol{L}(\hat{v}(s)) - \mathcal{P}_N \boldsymbol{N}(\hat{v}(s))\|$, is rather close to zero from zone III to zone V. It suggests that there is no action for the MAP from zone III to zone V and thus heteroclinic orbits for the K–S equation should exist from zone III to zone IV and from zone IV to zone V, if zones III–IV correspond to some non-equivalent saddle points.

(iii) The 'flat' part in zone V, see the right plot in figure 4, might correspond to a homoclinic orbit. The MAP in zone V is smooth, which implies that there exists dynamics. Only small fluctuations exist in this region means that the dynamics happens close to the translationally invariant set of saddle points.

We must mention that the obtained MAP is not accurate enough due to the complicated dynamics. For example, after zone V, the MAP should be a landing path to the travelling wave, which implies that the action in this part should be exactly zero. We have two problems here: (1) we need to truncate the time interval from $[-\infty, +\infty]$ to $[0, T]$; (2) trajectories locking onto the travelling wave are of infinite length, which implies that the MAP should also be of infinite length. The small action after $\hat{v}_{\mathrm{V}}$ is mainly due to the second problem, which is still a research topic, although enlarging T can improve the numerical results. However, such errors do not affect qualitatively the information we are looking for.

Table 1. Energy (E) and dimension (n_u) of unstable manifold of the saddle points.

	$\hat{v}_{\mathrm{I}}$	$\hat{v}_{\mathrm{II}}$	$\hat{v}_{\mathrm{III}}$	$\hat{v}_{\mathrm{IV}}$	$\hat{v}_{\mathrm{V}}$
n_u	1	2	6	4	2
E	8.9181	5.9922	0	7.6499	3.4640

We should also keep in mind that the obtained MAP may just correspond to a local minimum instead of a global one. Thus, we need to examine the obtained MAP carefully. A straightforward proposal consists of

- Locate the saddle points in zones I–V.
- Study the relations between those saddle points, i.e. we want to find out how their unstable manifolds connect to other structures.
- Study the relations between the attractors and saddle points, i.e. we want to find out the saddle points on the boundary of basin of attraction of the attractors, and identify the most probable exit point.

Once we obtain a more detailed picture with the above information, we will be able to tell whether the MAP we obtained is a local minimum or not. We will implement such a proposal and investigate the observations (i)–(iii) subsequently.

4.2.1. Allocate saddle points. We use a Newton solver to search fixed points in zones I–V using the points on the MAP as initial guesses. Five saddle points, up to a constant due to the translational invariance, are found. We order them from $\hat{v}_{\mathrm{I}}$ to $\hat{v}_{\mathrm{V}}$ corresponding to zones I–V. Note that $\hat{v}_{\mathrm{III}}$ is the trivial fixed point, which is not stable for $\alpha = 52$ demonstrated previously by the linear analysis. All saddle points have a centre manifold due to the translational invariance, except the trivial one $\hat{v}_{\mathrm{III}}$. For each saddle point, we implement linear analysis. In table 1 we give the energy $\|\hat{v}_i\|^2$, $i = I, \ldots, V$, and the number of eigenvalues with a positive real part. The saddle point $\hat{v}_{\mathrm{V}}$ takes a bimodal form, i.e. Fourier coefficients are nonzero only for modes $\exp(\mathrm{i}kx)$ with k being even. Such a bimodal fixed point is a global attractor when $22.50 \leqslant \alpha \leqslant 43$ [17]. $\hat{v}_{\mathrm{I}}$, $\hat{v}_{\mathrm{II}}$ and $\hat{v}_{\mathrm{IV}}$ have components in all modes. The profiles of all saddle points are given in figure 3. What we are interested in is that the effect of these saddle points on the transition between the stable fixed points $G(\hat{v}_{\mathrm{F}})$ and the travelling wave $\hat{v}_{\mathrm{TW}}$.

4.2.2. Relations between saddle points $\hat{v}_{\mathrm{I}} - \hat{v}_{\mathrm{V}}$. It is seen in figure 4 that $\hat{v}_{\mathrm{I}}$ is located in zone I, which is the first saddle point on the MAP starting from $\hat{v}_{\mathrm{F}}$. This implies that the saddle point $\hat{v}_{\mathrm{I}}$ might be of particular interest to the escape from the basin of attraction of $\hat{v}_{\mathrm{F}}$. Furthermore, we note, see table 1, that the energy, 8.9820, of the stable fixed point $\hat{v}_{\mathrm{F}}$, is only slightly different from the energy, 8.9181, of saddle point $\hat{v}_{\mathrm{I}}$. It is shown in table 1 that $\hat{v}_{\mathrm{I}}$ has one-dimensional unstable manifold. To characterize the unstable manifold of $\hat{v}_{\mathrm{I}}$, we look at the trajectories starting from around $\hat{v}_{\mathrm{I}}$. We introduce a small perturbation $\delta\hat{v}_{\mathrm{I}}$ along the tangent direction of the unstable manifold of $\hat{v}_{\mathrm{I}}$, which corresponds to the eigenvector associated with a positive eigenvalue, and compute the trajectories starting from $\hat{v}_{\mathrm{I}} + \delta\hat{v}_{\mathrm{I}}$ and $\hat{v}_{\mathrm{I}} - \delta\hat{v}_{\mathrm{I}}$. By varying the degree of perturbation ($\leqslant 1\%$), three types of trajectories are observed: starting from $\hat{v}_{\mathrm{I}} - \delta\hat{v}_{\mathrm{I}}$, the trajectory goes back to $\hat{v}_{\mathrm{F}}$; starting from $\hat{v}_{\mathrm{I}} + \delta\hat{v}_{\mathrm{I}}$, the trajectory goes to another stable fixed point $\tau_c\hat{v}_{\mathrm{F}}$ with $c \neq 0$, or to the travelling wave, depending on the size of $\delta\hat{v}$. In figure 5, we plot three typical trajectories starting from around $\hat{v}_{\mathrm{I}}$: the dotted, dashed and solid lines indicate trajectories locking onto $\hat{v}_{\mathrm{F}}$, $\tau_c\hat{v}_{\mathrm{F}}$ and the travelling wave, where $c \neq 0$.

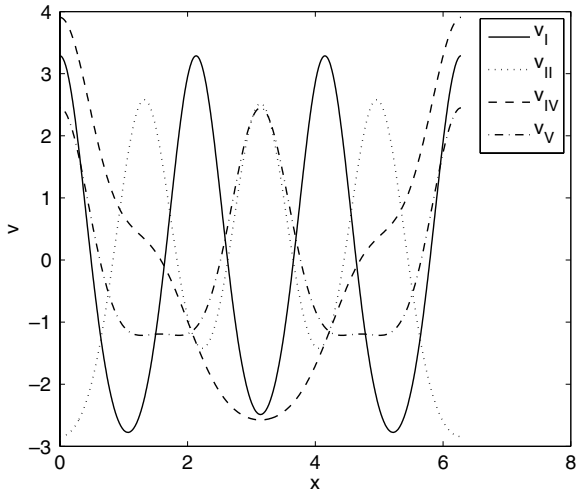

Figure 3. Profiles of $v_{\mathrm{I}}(x)$, $v_{\mathrm{II}}(x)$, $v_{\mathrm{IV}}(x)$ and $v_{\mathrm{V}}(x)$. Note here that we shift all periodic solutions along x-axis to make them even.

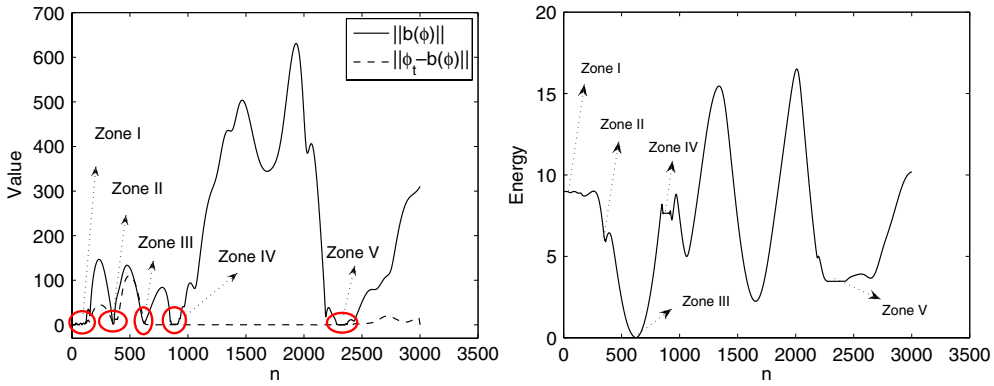

Figure 4. Left: forces and residuals at each point along the MAP. Right: energy at each point along the MAP.

(This figure is in colour only in the electronic version)

We now can conclude that the obtained MAP is indeed a local minimum. If we chop off the original MAP from $\hat{\boldsymbol{v}}_{\mathrm{F}}$ to $\hat{\boldsymbol{v}}_{\mathrm{I}}$ and combine this piece with the trajectory from $\hat{\boldsymbol{v}}_{\mathrm{I}}$ to the travelling wave, which was found above by analysing the unstable manifold of $\hat{\boldsymbol{v}}_{\mathrm{I}}$, we obtain a new MAP, starting from $\hat{\boldsymbol{v}}_{\mathrm{F}}$ and ending at $\hat{\boldsymbol{v}}_{\mathrm{TW}}$. This new MAP has a much smaller action than the original one, which is 0.2754 in contrast to 365.1478, the action associated with the old MAP. Note here that numerical experiments show that the convergence of MAP to a certain local minimum is mainly determined by the initial guess of MAP, not by the temporal discretization in the aMAM.

The flat part in the left plot of figure 5 implies that trajectories from $\hat{\boldsymbol{v}}_{\mathrm{I}} + \delta\hat{\boldsymbol{v}}_{\mathrm{I}}$ to $\tau_c\hat{\boldsymbol{v}}_{\mathrm{F}}$ or $\hat{\boldsymbol{v}}_{\mathrm{TW}}$ will stay for a long time around a state with energy 3.4640, before locking onto $\tau_c\hat{\boldsymbol{v}}_{\mathrm{F}}$ or $\hat{\boldsymbol{v}}_{\mathrm{TW}}$. From table 1, we know that such a state corresponds to $\hat{\boldsymbol{v}}_{\mathrm{V}}$ or its translational images $\tau_c\hat{\boldsymbol{v}}_{\mathrm{V}}$. The sensitivity of these trajectories to the initial conditions, as well as the long time

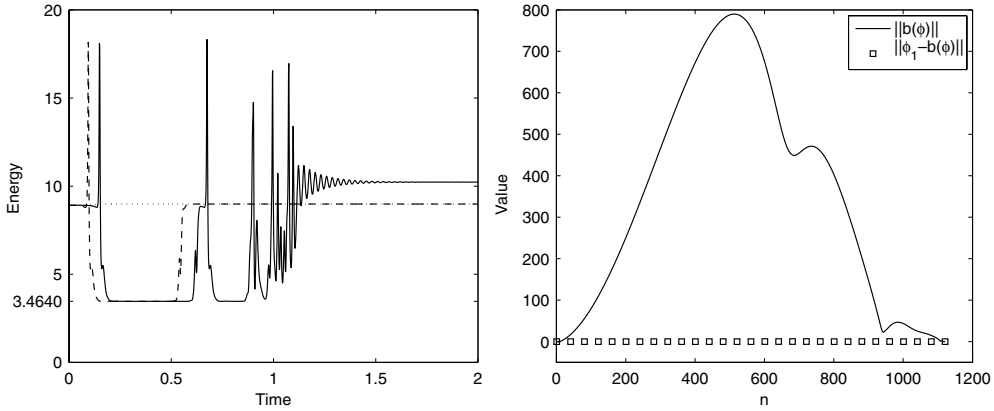

Figure 5. Left: energy of trajectories starting from the vicinity of $\hat{v}_{\mathrm{I}}$. The solid, dash and dotted lines indicate the trajectories landing onto $\hat{v}_{\mathrm{TW}}$, $\tau_c\hat{v}_{\mathrm{F}}$ and $\hat{v}_{\mathrm{F}}$, respectively; Right: a heteroclinic orbit exists between saddle points $\hat{v}_{\mathrm{I}}$ and $\hat{v}_{\mathrm{V}}$.

excursion at the energy level of $\hat{v}_{\mathrm{V}}$, implies there may exist a heteroclinic orbit from $\hat{v}_{\mathrm{I}}$ to $\hat{v}_{\mathrm{V}}$ or one of its translational images. It is usually not easy to obtain numerically such a heteroclinic orbit by just testing different initial conditions around $\hat{v}_{\mathrm{I}}$ along its unstable manifold, since $\hat{v}_{\mathrm{V}}$ is not stable. However, using the fact that the action functional along a heteroclinic orbit is zero, we can use aMAM to test if the corresponding MAP has zero action. If so, the obtained MAP must be the heteroclinic orbit we are looking for. Specifically, we solve the optimization problem (15) subject to the following constraints

$$\hat{v}(0) = \hat{v}_{\mathrm{I}}, \qquad \hat{v}(T) = \tau_c\hat{v}_{\mathrm{V}} \in \tau(\hat{v}_{\mathrm{V}}),$$

where c is free and $\hat{v}_{\mathrm{V}}$ is a point given by the Newton solver. Note here that we need to use $\tau_c\hat{v}_{\mathrm{V}}$ as the endpoint of MAP to let the optimization algorithm also minimize c.

The initial guess of MAP for the above problem should be carefully chosen to avoid being trapped in a local minimum. We can use the trajectory in the left plot of figure 5 which starts from $\hat{v}_{\mathrm{I}} + \delta\hat{v}_{\mathrm{I}}$ and makes excursion at the energy level of $\hat{v}_{\mathrm{V}}$. We truncate this trajectory at a point which has the closest energy to that of $\hat{v}_{\mathrm{V}}$ or the minimal distance to the set $\tau(\hat{v}_{\mathrm{V}})$. The values of $\|\mathcal{P}_N\boldsymbol{L}(\hat{v}(s)) + \mathcal{P}_N\boldsymbol{N}(\hat{v}(s))\|$ and $\|\dot{\hat{v}}(s) - \mathcal{P}_N\boldsymbol{L}(\hat{v}(s)) - \mathcal{P}_N\boldsymbol{N}(\hat{v}(s))\|$ along the obtained MAP for this case are given in the right plot of figure 5. The zero action from $\hat{v}_{\mathrm{I}}$ to $\tau_c\hat{v}_{\mathrm{V}}$ implies that the obtained MAP is indeed the heteroclinic orbit.

Another interesting observation in the left plot of figure 5 is that before eventually locking onto the travelling wave, the trajectory first stays around $\tau_c\hat{v}_{\mathrm{V}}$, then *bursts* away and comes back to the same energy level and then jumps back and forth to a state of constant energy. This phenomenon was reported and discussed in [17], which confirmed that there exists a homoclinic orbit from $\hat{v}_{\mathrm{V}}$ to $\tau_c\hat{v}_{\mathrm{V}}$. The observation is consistent with our conjecture (iii) (see section 4.2) based on the information of the MAP. In figure 6, we give a schematic of the unstable manifold of $\hat{v}_{\mathrm{I}}$ and $\hat{v}_{\mathrm{V}}$. $\hat{v}_{\mathrm{I}}$ has one positive eigenvalue, and a heteroclinic orbit exists from $\hat{v}_{\mathrm{I}}$ to $\hat{v}_{\mathrm{V}}$. $\hat{v}_{\mathrm{V}}$ has two conjugate eigenvalues with a positive real part. Its unstable manifold is connected to some translational images of $\hat{v}_{\mathrm{F}}$, $\hat{v}_{\mathrm{V}}$ and the travelling wave.

It is clear that the original MAP in figure 4 tells us that there exists heteroclinic orbits from $\hat{v}_{\mathrm{III}}$ to $\hat{v}_{\mathrm{IV}}$ and from $\hat{v}_{\mathrm{IV}}$ to $\hat{v}_{\mathrm{V}}$ due to the corresponding zero actions. However, the MAP does not tell us much about the unstable manifold of $\hat{v}_{\mathrm{II}}$. We subsequently examine $\hat{v}_{\mathrm{II}}$. We would like to use this case as an example to demonstrate that the MAM is a helpful technique

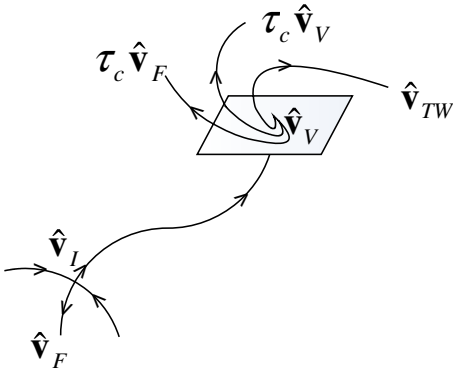

Figure 6. Schematic of the unstable manifold of $\hat{v}_{\mathrm{I}}$ and $\hat{v}_{\mathrm{V}}$.

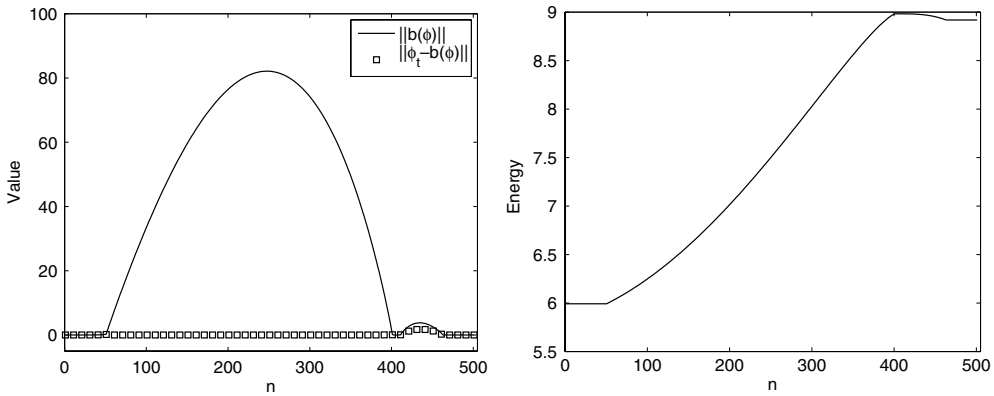

Figure 7. Information of the MAP from $\hat{v}_{\mathrm{II}}$ to $\hat{v}_{\mathrm{I}}$ starting from a linear initial path. Left: force and residual at each point along the MAP. Right: energy at each point along the MAP.

tool to study the phase space when a saddle point has a high dimensional unstable manifold. Actually we will see later in figure 11 that the MAP from $\hat{v}_{\mathrm{TW}}$ to $\tau_c \hat{v}_{\mathrm{F}}$ shows that there exists a heteroclinic orbit from $\hat{v}_{\mathrm{II}}$ to $\hat{v}_{\mathrm{I}}$. $\hat{v}_{\mathrm{II}}$ has two distinct positive eigenvalues. Let $\delta_1 \hat{v}_{\mathrm{II}}$ and $\delta_2 \hat{v}_{\mathrm{II}}$ denote the perturbation along the corresponding eigenvectors, where the eigenvalue for $\delta_1 \hat{v}_{\mathrm{II}}$ is larger than that for $\delta_2 \hat{v}_{\mathrm{II}}$. Numerical experiments show that the trajectories starting from $\hat{v}_{\mathrm{II}} \pm \delta_1 \hat{v}_{\mathrm{II}}$ and $\hat{v}_{\mathrm{II}} - \delta_2 \hat{v}_{\mathrm{II}}$ go to the travelling wave and the trajectory starting from $\hat{v}_{\mathrm{II}} + \delta_2 \hat{v}_{\mathrm{II}}$ goes to a stable fixed point. However, this means that if the initial condition changes gradually from $\hat{v}_{\mathrm{II}} \pm \delta_1 \hat{v}_{\mathrm{II}}$ or $\hat{v}_{\mathrm{II}} - \delta_2 \hat{v}_{\mathrm{II}}$ to $\hat{v}_{\mathrm{II}} + \delta_2 \hat{v}_{\mathrm{II}}$ along a circle around $\hat{v}_{\mathrm{II}}$ on its two-dimensional unstable manifold, the solution will have to jump from the travelling wave to a stable fixed point. Such a fundamental change in the solutions implies that a heteroclinic orbit should exist from $\hat{v}_{\mathrm{II}}$ to a certain saddle point. To verify this, we need to look at the MAPs from $\hat{v}_{\mathrm{II}}$ to all other saddle points. Although none of them give a MAP with zero action, in other words, a global minimum is not obtained, the MAP from $\hat{v}_{\mathrm{II}}$ to $\hat{v}_{\mathrm{I}}$ shows properties consistent with the above observations. In figure 7, we plot the information of the obtained MAP using the linear path as an initial guess. In the left plot of figure 7, we see that there exist two caps in the curve $\|\mathcal{P}_N \boldsymbol{L}(\hat{v}(s)) + \mathcal{P}_N \boldsymbol{N}(\hat{v}(s))\|$, and one fixed point connecting these two caps. According to the energy curve, we know that such a fixed point is a stable one. Thus, the MAP is trapped to a

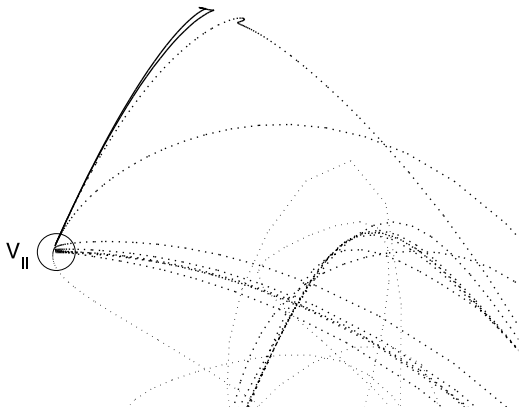

Figure 8. Trajectories starting from points on the MAP, which are close to the saddle point $\hat{v}_{\mathrm{II}}$.

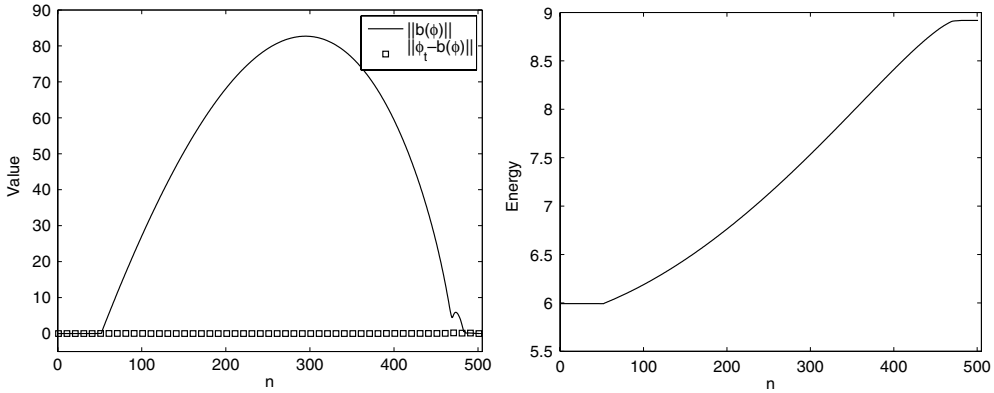

Figure 9. There exists a heteroclinic orbit from $\hat{v}_{\mathrm{II}}$ to $\tau_c(\hat{v}_{\mathrm{I}})$. Left: force and residual at each point along the MAP. Right: energy at each point along the MAP.

stable fixed point before it goes to $\hat{v}_{\mathrm{I}}$. We then use the points on the MAP, which are close to $\hat{v}_{\mathrm{II}}$, as initial conditions and track their evolution. In figure 8, we plot (part of) these trajectories, where all the dotted trajectories will finally lock onto the travelling wave, and the two solid trajectories go to stable fixed points. This exactly corresponds to what we have observed in the perturbation analysis. We also observe that some trajectories go to $\hat{v}_{\mathrm{I}}$ first before they make a sharp turn to diverge. We now know qualitatively that there exists a heteroclinic orbit from $\hat{v}_{\mathrm{II}}$ to $\hat{v}_{\mathrm{I}}$. However, to obtain this heteroclinic orbit, we need a better initial path, e.g. part of the dotted trajectory which is closest to the solid ones in figure 8. In figure 9, we give the information of the heteroclinic orbit from $\hat{v}_{\mathrm{II}}$ to $\tau_c\hat{v}_{\mathrm{I}}$. We see that the stable fixed point disappears and the energy increases monotonically to that of $\hat{v}_{\mathrm{I}}$. We note here that it is important to use the points on the MAP as the initial conditions, since it is difficult to choose a good initial MAP by sampling when the unstable manifold is high dimensional.

4.2.3. The transition from $\hat{v}_{\mathrm{F}}$ to $\hat{v}_{\mathrm{TW}}$. We now summarize the transition from the stable fixed point $\hat{v}_{\mathrm{F}}$ to the travelling wave $\hat{v}_{\mathrm{TW}}$. The MAP given by the numerical optimization is

$$\hat{v}_{\mathrm{F}} \to \tau_c\hat{v}_{\mathrm{I}} \to \tau_c\hat{v}_{\mathrm{II}} \to \tau_c\hat{v}_{\mathrm{III}} \to \tau_c\hat{v}_{\mathrm{IV}} \to \tau_c\hat{v}_{\mathrm{V}} \to \hat{v}_{\mathrm{TW}},$$

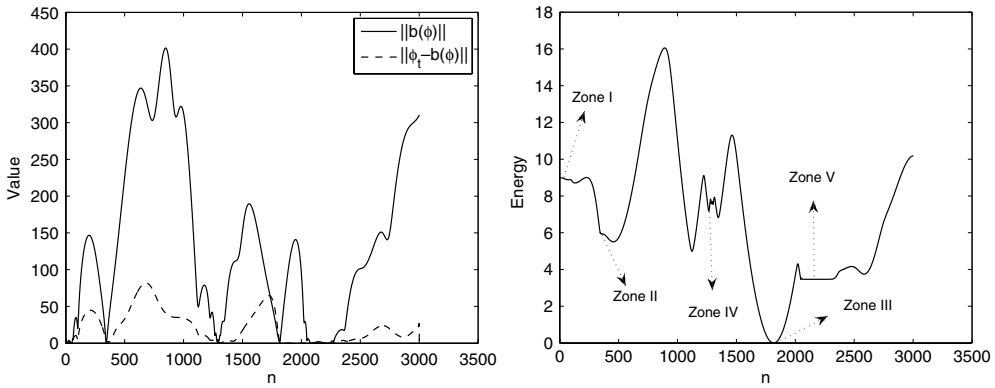

Figure 10. Information of the MAP from $\tilde{\hat{v}}_{\mathrm{F}}$ to $\hat{v}_{\mathrm{TW}}$ starting from a linear initial path. Left: force and residual at each point along the MAP. Right: energy at each point along the MAP. The ordering of the zones follows that in figure 4.

where c is a general constant. We know this is only a local minimum, and the most probable transition path should be

$$\hat{v}_{\mathrm{F}} \to \tau_c \hat{v}_{\mathrm{I}} \to \tau_c \hat{v}_{\mathrm{V}} \to \text{homoclinic orbit} \to \hat{v}_{\mathrm{TW}}. \tag{21}$$

Here, the 'homoclinic orbit' means the orbit connecting two equivalent solutions in the set $\tau(\hat{v}_{\mathrm{V}})$.

Thus, $\hat{v}_{\mathrm{I}}$ is the most probable first exit point for the escape from the basin of attraction of $\hat{v}_{\mathrm{F}}$ and the MAP from $\hat{v}_{\mathrm{F}}$ to $\hat{v}_{\mathrm{I}}$ is the most probable exit path. We note that any translational image of $\hat{v}_{\mathrm{I}}$, except itself, is not the most probable exit point which has the least action, for the problem of escape from the basin of attraction of $\hat{v}_{\mathrm{F}}$. To test this, we compute the MAP from $\hat{v}_{\mathrm{F}}$ to $\tau_c \hat{v}_{\mathrm{I}}$ for some $c \neq 0$. Numerical results show that $c = 0$ is optimal, i.e. the action from $\hat{v}_{\mathrm{F}}$ to $\hat{v}_{\mathrm{I}}$ is the smallest one.

As we remarked previously that if we translate the initial state to $\tau_c \hat{v}_{\mathrm{F}}$, the transition pathway in (21) should be robust due to translational invariance of the K–S equation. As a numerical verification, let $\tilde{\hat{v}}_{\mathrm{F}}$ be a translational image of $\hat{v}_{\mathrm{F}}$, such as the stable point that $\hat{v}_{\mathrm{I}} + \delta \hat{v}_{\mathrm{I}}$ converges to (see section 4.2.2). We calculate the MAP from $\tilde{\hat{v}}_{\mathrm{F}}$ to $\hat{v}_{\mathrm{TW}}$ starting from a linear initial path. Basically a similar story happens here. From figure 10, we see that the MAP converges to a local minimum

$$\tilde{\hat{v}}_{\mathrm{F}} \to \tau_c \hat{v}_{\mathrm{I}} \to \tau_c \hat{v}_{\mathrm{II}} \to \tau_c \hat{v}_{\mathrm{IV}} \to \tau_c \hat{v}_{\mathrm{III}} \to \tau_c \hat{v}_{\mathrm{V}} \to \hat{v}_{\mathrm{TW}},$$

where c is a general constant. The only difference from the MAP from $\hat{v}_{\mathrm{F}}$ to $\hat{v}_{\mathrm{TW}}$ is that $\tau_c \hat{v}_{\mathrm{IV}}$ and $\tau_c \hat{v}_{\mathrm{III}}$ are switched with each other. It is seen that the most probable escape path from the basin of attraction of $\tilde{\hat{v}}_{\mathrm{F}}$ takes a saddle point $\tau_c \hat{v}_{\mathrm{I}}$ which is just a translational image of the original transition state $\hat{v}_{\mathrm{I}}$. So, the transition pattern (21) is valid for all equivalent solutions of $\hat{v}_{\mathrm{F}}$. In addition, as a byproduct observed in figure 10, we note that the MAP from $\tilde{\hat{v}}_{\mathrm{F}}$ to $\hat{v}_{\mathrm{TW}}$ tells that there exists a heteroclinic orbit from $\hat{v}_{\mathrm{III}}$ and $\tau_c \hat{v}_{\mathrm{V}}$.

4.3. Experiment II—from $\hat{v}_{\mathrm{TW}}$ to $G(\hat{v}_{\mathrm{F}})$

To study the escape from the basin of attraction of $\hat{v}_{\mathrm{TW}}$, we consider the constraints

$$\hat{v}(0) = \hat{v}_{\mathrm{TW}}, \qquad \hat{v}(T) = \tau_c \hat{v}_{\mathrm{F}} \in \tau(\hat{v}_{\mathrm{F}}).$$

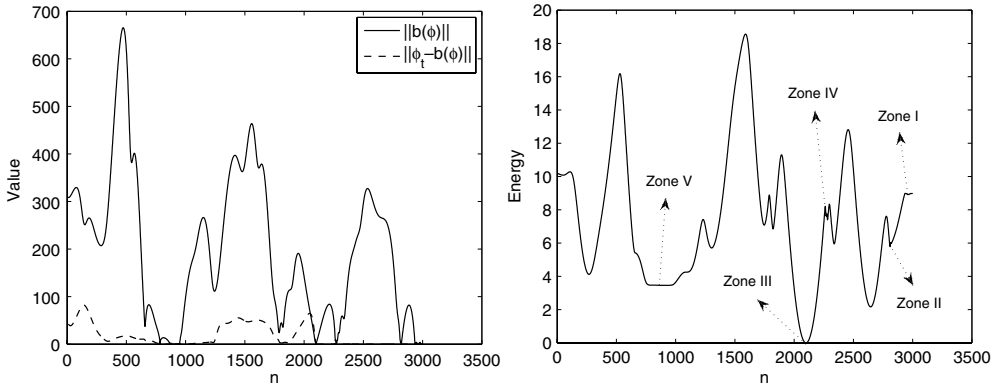

Figure 11. Information of the MAP from $\hat{v}_{\mathrm{TW}}$ to $\hat{v}_{\mathrm{F}}$ starting from a linear initial path. Left: forces and residuals at each point along the MAP. Right: energy at each point along the MAP. The ordering of the zones corresponds to that in figure 4.

for the optimization problem (15). The information of the obtained MAP is shown in figure 11. We see that the MAP takes a transition pattern

$$\hat{v}_{\mathrm{TW}} \to \tau_c \hat{v}_{\mathrm{V}} \to \tau_c \hat{v}_{\mathrm{III}} \to \tau_c \hat{v}_{\mathrm{IV}} \to \tau_c \hat{v}_{\mathrm{II}} \to \tau_c \hat{v}_{\mathrm{I}} \to \tau_c(\hat{v}_{\mathrm{F}}).$$

No new saddle points show up. The MAP implies that there exist heteroclinic orbits from $\hat{v}_{\mathrm{III}}$ to $\hat{v}_{\mathrm{IV}}$, from $\hat{v}_{\mathrm{IV}}$ to $\hat{v}_{\mathrm{II}}$, and from $\hat{v}_{\mathrm{II}}$ to $\hat{v}_{\mathrm{I}}$. However, if we zoom into the part of MAP from $\hat{v}_{\mathrm{II}}$ to $\hat{v}_{\mathrm{I}}$, we will see that the MAP will be trapped by a stable fixed point before reaching $\hat{v}_{\mathrm{I}}$ as observed in figure 7. We summarize all known heteroclinic orbits in figure 12.

It can be seen that all the saddle points are on the boundary of basin of attraction of the travelling wave. Recall that the trajectories starting around $\hat{v}_{\mathrm{V}}$ can also go to $G(\hat{v}_{\mathrm{F}})$. Starting from any saddle point, a zero MAP can be constructed to either $G(\hat{v}_{\mathrm{F}})$ or the travelling wave using the heteroclinic orbits described in figure 12. In other words, all the saddle points can be a possible choice for the escape from basin of attraction of the travelling wave. However, among all five saddle points $\hat{v}_i$, $i = I, \ldots, V$, only $\hat{v}_{\mathrm{I}}$ is of index-1 type, i.e. the unstable manifold is one dimensional. Such a scenario is completely different from the gradient dynamical systems. The MAM picks the saddle point $\tau_c \hat{v}_{\mathrm{V}}$, implying the transition pattern should be

$$\hat{v}_{\mathrm{TW}} \to \tau_c \hat{v}_{\mathrm{V}} \to G(\hat{v}_{\mathrm{F}}).$$

Such a result can be further verified by computing the MAP between the travelling wave and other saddle points and considering the relations between saddle points given in figure 12. Numerical results are omitted here. The discovery that $\hat{v}_{\mathrm{V}}$ or its translational image is the transition state may suggest that when one studies important unstable states or patterns on the basin boundary in general non-gradient dynamical systems, such as the notion of 'edge state' [25, 26] in the study of turbulence transition, one should also pay attention to fixed points which are not a relative attractor, but have index number $\geqslant 2$. Although all flows on the basin boundary will eventually go to some relative attractors on the basin boundary, it is possible that the noise-induced transition may select other types of fixed points as transition states [27].

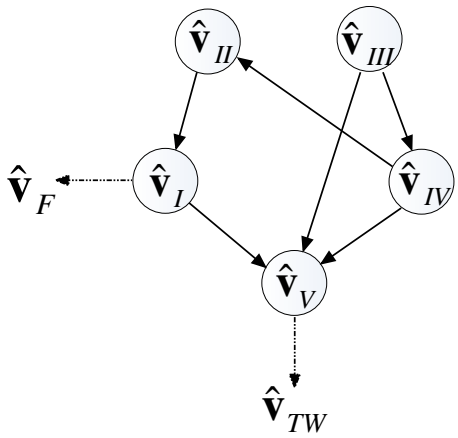

Figure 12. Diagram for hetereclinic orbits between saddle points $\hat{v}_{\mathrm{I}} - \hat{v}_{\mathrm{V}}$, where the hetereclinic orbits are indicated by directed solid lines.

5. Summary

The noise-induced transitions between a stable fixed point and a stable travelling wave are studied for the stochastic K–S equation. Five saddle points on the basin boundary are found. Not only their connections but also their roles in the noise-induced transitions are clarified. Our approach relies on the framework of Wentzell–Freidlin large deviation principle and the numerical tool of aMAM.

Compared with other similar work on breaking the complicated phase space into a few 'low dimensional inertial manifold', such as [28], our approach of the MAM has a few different features. First, we only need the information of two attractors and no other prior information or preprocessing (such as edge tracking to search along the basin boundary) is required. Most optimization algorithms only guarantee to find a local minimum instead of the global one. Nevertheless, the MAP we obtain does give us some fixed points or the region where the dynamics $|b|$ is slow. Thus, the information of the MAP directly provides us some very good initial guesses for Newton-type algorithms to locate saddle points exactly. We should mention that one single MAP typically finds most of the relevant saddle points, instead of searching them one bye one in a very local way. Furthermore, by looking at the value of the Wentzell–Freidlin action (also called quasi-potential or non-equilibrium potential in physical literature) of different saddle fixed points, we can rigorously quantify the instability related to them when the dynamical system is perturbed by a small noise and find the most probable exit point, i.e. the one with the least action value on the basin boundary. Such a viewpoint can provide a perspective to evaluate the importance of unstable solutions or patterns where the long time dynamics is considered.

In this work, we focused on the search for unstable fixed points along the MAP. However, limit cycles can also play an important role in transitions [12]. How to use the MAM to deal with the case of limit cycles [29, 30] is also an interesting and important topic. The study in this direction will be reported elsewhere.

Acknowledgments

This work is supported by AFOSR grant FA9550-08-1-0433 and ONR grant N00014-01-1-0674.

Appendix A. Numerical schemes for equation (13)

Let $\tilde{\boldsymbol{L}} = \mathcal{P}_N \boldsymbol{L}$ and $\tilde{\boldsymbol{N}} = \mathcal{P}_N \boldsymbol{N}$. The ODE system (13) can be rewritten as

$$\frac{d(\mathrm{e}^{-\tilde{\boldsymbol{L}}t}\tilde{\boldsymbol{v}})}{dt} = \mathrm{e}^{-\tilde{\boldsymbol{L}}t}\tilde{\boldsymbol{N}}(\tilde{\boldsymbol{v}}, t). \tag{A.1}$$

Coupling the fourth-order Runge–Kutta scheme, the following ETD scheme was given in [31]:

$$\boldsymbol{a}_k = \mathrm{e}^{\tilde{\boldsymbol{L}}h/2}\tilde{\boldsymbol{v}}_k + \tilde{\boldsymbol{L}}^{-1}(\mathrm{e}^{\tilde{\boldsymbol{L}}h/2} - \boldsymbol{I})\tilde{\boldsymbol{N}}(\tilde{\boldsymbol{v}}_k, t_k),$$

$$\boldsymbol{b}_k = \mathrm{e}^{\tilde{\boldsymbol{L}}h/2}\tilde{\boldsymbol{v}}_k + \tilde{\boldsymbol{L}}^{-1}(\mathrm{e}^{\tilde{\boldsymbol{L}}h/2} - \boldsymbol{I})\tilde{\boldsymbol{N}}(\boldsymbol{a}_k, t_k + h/2),$$

$$\boldsymbol{c}_k = \mathrm{e}^{\tilde{\boldsymbol{L}}h/2}\boldsymbol{a}_k + \tilde{\boldsymbol{L}}^{-1}(\mathrm{e}^{\tilde{\boldsymbol{L}}h/2} - \boldsymbol{I})(2\tilde{\boldsymbol{N}}(\boldsymbol{b}_k, t_k + h/2) - \tilde{\boldsymbol{N}}(\tilde{\boldsymbol{v}}_k, t_k)),$$

$$\begin{aligned}\tilde{\boldsymbol{v}}_{k+1} = {} & \mathrm{e}^{\tilde{\boldsymbol{L}}h}\tilde{\boldsymbol{v}}_k + h^{-2}\tilde{\boldsymbol{L}}^{-3}\{[-4 - \tilde{\boldsymbol{L}}h + \mathrm{e}^{\tilde{\boldsymbol{L}}h}(4 - 3\tilde{\boldsymbol{L}}h + (\tilde{\boldsymbol{L}}h)^2)]\tilde{\boldsymbol{N}}(\tilde{\boldsymbol{v}}_k, t_k) \\ & + 2[2 + \tilde{\boldsymbol{L}}h + \mathrm{e}^{\tilde{\boldsymbol{L}}h}(-2 + \tilde{\boldsymbol{L}}h)](\tilde{\boldsymbol{N}}(\boldsymbol{a}_k, t_k + h/2) + \tilde{\boldsymbol{N}}(\boldsymbol{b}_k, t_k + h/2)) \\ & + [-4 - 3\tilde{\boldsymbol{L}}h - (\tilde{\boldsymbol{L}}h)^2 + \mathrm{e}^{\tilde{\boldsymbol{L}}h}(4 - \tilde{\boldsymbol{L}}h)]\tilde{\boldsymbol{N}}(\boldsymbol{c}_k, t_k + h)\}.\end{aligned}$$

To enhance the robustness, $g(\tilde{\boldsymbol{L}}) = \tilde{\boldsymbol{L}}^{-1}(\mathrm{e}^{\tilde{\boldsymbol{L}}h}/2 - \boldsymbol{I})$ is evaluated via an integral over a contour Γ [23]:

$$g(\tilde{\boldsymbol{L}}) = \frac{1}{2\pi \mathrm{i}} \int_{\Gamma} g(t)(t\boldsymbol{I} - \tilde{\boldsymbol{L}})^{-1} dt, \tag{A.2}$$

where Γ can be any contour that encloses the eigenvalues of $\tilde{\boldsymbol{L}}$.

References

[1] Karmers H A 1940 Brownian motion in a field of force and the diffusion model of chemical reactions *Physica* **7** 284–304

[2] Van Kampen N G 1981 *Stochastic Processes in Physics and Chemistry* (Amsterdam: North-Holland)

[3] Wales D J 2003 *Energy Landscapes with Application to Clusters, Biomolecules and Glasses* (Cambridge: Cambridge University Press)

[4] Onsager L and Machlup S 1953 Fluctuations and irreversible processes *Phys. Rev.* **91** 1505–12

[5] Ren W 2002 Numerical methods for the study of energy landscape and rare events *PhD Thesis* New York University

[6] E W, Ren W and Vanden-Eijnden E 2002 String method for the study of rare events *Phys. Rev.* B **66** 052301

[7] E W, Ren W and Vanden-Eijnden E 2007 Simplified and improved string method for computing the minimum energy paths in barrier-crossing events *J. Chem. Phys.* **126** 164103

[8] Jònsson H, Mills G and Jacobsen K W 1998 Nudged elastic band method for finding minimum energy paths of transitions *Classical and Quantum Dynamics in Condensed Phase Simulations* (*LERICI, Villa Marigola*) *Proc. of the Int. School of Physics* ed B J Berne *et al* (Singapore: World Scientific) p 385

[9] Cerjan C J and Miller W H 1981 On finding transition states *J. Chem. Phys.* **75** 2800–6

[10] Henkelman G and Jónsson H 1999 A dimer method for finding saddle points on high dimensional potential surfaces using only first derivatives *J. Chem. Phys.* **111** 7010–22

[11] Ren W, E W and Vanden-Eijnden E 2003 Energy landscape and thermally activated switching of submicro-sized ferromagnetic elements *J. Appl. Phys.* **93** 2275

[12] Zhou X and E W 2009 Study of noise-induced transitions in the Lorenz system using the minimum action method *Commun. Math. Sci.* **7** 341–55

[13] Zhou X 2009 Noise-induce transition pathway in non-gradient systems *PhD Thesis* Princeton University

[14] Kuramoto Y 1978 Diffusion-induced chaos in reactions systems *Suppl. Prog. Theor. Phys.* **64** 346–67

[15] Sivashinsky G 1977 Nonlinear analysis of hydrodynamic instability in laminar flames: I. Deviation of basic equations *Acta Astron.* **4** 1177–206

[16] Holmes P, Lumley J L and Berkooz G 1998 *Turbulence, Coherent Structures, Dynamical Systems and Symmetry* (*Cambridge Monographs on Mechanics*) (Cambridge: Cambridge University Press)

[17] Hyman J M and Nicolaenko B 1986 The Kuramoto–Sivashinsky equation: a bridge between PDE's and dynamical systems *Physics* D **18** 113–26
[18] E W, Ren W and Vanden-Eijnden E 2004 Minimum action method for the study of rare events *Commun. Pure Appl. Math.* **57** 637–56
[19] Freidlin M I and Wentzell A D 1998 Random perturbations of dynamical systems *Grundlehren der Mathematischen Wissenschaften* 2 edn (New York: Springer)
[20] Zhou X, Ren W and E W 2008 Adaptive minimum action method for the study of rare events *J. Chem. Phys.* **128** 104111
[21] Varadhan S R S 1984 *Large Deviations and Applications* (PA: SIAM)
[22] Foias C, Nicolaenko B, Sell G R and Temam R 1988 Inertial manifolds for the Kuramoto–Sivashinsky equation and an estimate of their lowest dimensions *J. Math. Pures Appl.* **67** 197–226
[23] Kassam A-K and Trefethen L N 2005 Fourth-order time-stepping for stiff PDEs *SIAM J. Sci. Comput.* **26** 1214–33
[24] Hager W W and Zhang H 2005 A new conjugate gradient method with guaranteed descent and an efficient line search *SIAM J. Optim.* **16** 170–92
[25] Skufca J D, Yorke J A and Eckhardt B 2006 Edge of chaos in a parallel shear flow *Phys. Rev. Lett.* **96** 174101
[26] Schneider T M, Eckhardt B and Yorke J A 2007 Turbulence transition and the edge of chaos in pipe flow *Phys. Rev. Lett.* **99** 034502
[27] Maier R S and Stein D L 1993 Escape problem for irreversible systems *Phys. Rev.* E **48** 931–8
[28] Gibson J F, Halcrow J and Cvitanovic P 2008 Visualizing the geometry of state space in plane couette flow *J. Fluid Mech.* **611** 107
[29] Lan Y 2008 Unstable recurrent patterns in Kuramoto–Sivashinsky dynamics *Phys. Rev.* E **78** 026208
[30] Kawahara G and Kida S 2001 Periodic motion embedded in plane couette turbulence: regeneration cycle and burst *J. Fluid Mech.* **449** 291–300
[31] Cox S M and Matthews P C 2002 Exponential time differencing for stiff systems *J. Comput. Phys.* **176** 430–55